Excitations of amorphous solid helium

Jacques Bossy,[1] Jacques Ollivier,[2] Helmut Schober,[2,3] and H. R. Glyde[4]
[1]*Institut Néel, CNRS-UJF, BP 166, 38042 Grenoble Cedex 9, France*
[2]*Institut Laue-Langevin, BP 156, 38042 Grenoble, France*
[3]*Université Joseph Fourier, UFR de Physique, F38041 Grenoble Cedex 9, France*
[4]*Department of Physics and Astronomy, University of Delaware, Newark, Delaware 19716-2593, USA*
(Received 24 August 2012; revised manuscript received 14 October 2012; published 7 December 2012)

We present neutron scattering measurements of the dynamic structure factor $S(Q,\omega)$ of amorphous solid helium confined in 47-Å pore diameter MCM-41 at pressure 48.6 bars. At low temperature $T = 0.05$ K, we observe $S(Q,\omega)$ of the confined quantum amorphous solid plus the bulk polycrystalline solid between the MCM-41 powder grains. No liquidlike phonon-roton modes, other sharply defined modes at low energy ($\omega < 1.0$ meV), or modes unique to a quantum amorphous solid that might suggest superflow are observed. Rather, the $S(Q,\omega)$ of confined amorphous and bulk polycrystalline solid appear to be very similar. At higher temperature ($T > 1$ K), the amorphous solid in the MCM-41 pores melts to a liquid which has a broad $S(Q,\omega)$ peaked near $w \simeq 0$, characteristic of normal liquid ^{4}He under pressure. Expressions for the $S(Q,\omega)$ of amorphous and polycrystalline solid helium are presented and compared. In previous measurements of liquid ^{4}He confined in MCM-41 at lower pressure, the intensity in the liquid roton mode decreases with increasing pressure until the roton vanishes at the solidification pressure (38 bars), consistent with no roton in the solid observed here.

DOI: 10.1103/PhysRevB.86.224503 PACS number(s): 67.80.bd, 67.80.de, 67.25.dr, 61.05.F−

I. INTRODUCTION

The superfluid fraction of liquid ^{4}He, both bulk and ^{4}He in porous media, is traditionally and most accurately measured in a torsional oscillator (TO). Below a critical temperature T_c, the TO frequency increases, indicating that a fraction of the helium mass has decoupled and ceased to rotate with the TO. The effect is denoted a nonclassical rotational inertia (NCRI) and the decoupled fraction is identified as the superfluid fraction.

In 2004, Kim and Chan[1,2] reported a similar NCRI in solid ^{4}He, in both bulk solid[1] and in solid ^{4}He confined in Vycor.[2] Remarkably, below a $T_c \simeq$ 200 mK, a small fraction of the solid apparently decouples in a TO. The NCRI has now been widely reproduced in other laboratories in a variety of sample cells.[3–9] However, the magnitude of the NCRI observed varies between 0 and 1.5%, depending on how the sample is prepared, quenched, or annealed, on the ^{3}He concentration and on other factors. This suggests that the NCRI is associated with defects in the solid, dislocations, grain boundaries, amorphous regions, or other defects.[10–13] The magnitude and character of the NCRI depends on the oscillator frequency[7,8,14] and shows effects[15–17] not usually associated with superflow. For example, the NCRI is associated with substantial elastic energy dissipation in the solid described by the Q of the oscillator. Indeed, in some cases, the observed frequency shift Δf and the dissipation ΔQ can be quite well described by the real and imaginary parts of a common dynamic susceptibility[15] as found in purely glassy systems.[15–17]

Day and Beamish[18,19] and others[20] have shown that the shear modulus μ of solid helium increases at low temperature with both a temperature dependence and a dependence on ^{3}He concentration that tracks that of the observed NCRI. The increase in μ is attributed to the stiffening of the solid as dislocations become pinned by ^{3}He at low temperature. A key question is whether the Δf can be entirely attributed to elastic behavior or whether there is some remaining part that must arise from other effects such as superflow.

Pursuing this question, Maris[21] and Beamish and co-workers[22] have shown that in some TOs there is sufficient solid helium in the torsional rod to explain the observed Δf completely in terms of elastic stiffening of the solid in the rod. However, in many others it can not,[22] and at least part of the observed Δf must have some other origin. Similarly, Choi and co-workers,[23,24] using a TO which includes dc rotation have shown that the critical velocity depends on the dc velocity as expected for genuine superflow. Thus, while the stiffening of the shear modulus below T_c and elastic effects can account for the Δf and ΔQ in some cases, it can not account for Δf in all cases[1,2,9,23,25] nor all effects.[23,24,26]

Path-integral Monte Carlo calculations predict that the superfluid fraction and Bose-Einstein condensate fraction in perfect crystalline solid helium are negligibly small.[27–29] However, a finite and observable superfluid fraction and condensate fraction is predicted[28] in amorphous solid helium. The first one to two layers of helium on rough porous media walls are amorphous. Typically, the solid in porous media grows from the amorphous layers inward toward the center of the pores.[30] In Vycor and aerogel, the tightly bound amorphous layers give way to crystalline solid after a few layers so that the solid in the interior of the pore is crystalline. However, if the pore size is small enough, the solid is amorphous throughout the pore, as predicted for classical solids.[31] Specifically, in 47-Å pore diameter MCM-41 and 34-Å pore diameter gelsil, we have shown[32] that the entire solid is amorphous (no Bragg peaks). Since superflow in amorphous solid ^{4}He is predicted, it is interesting to determine whether the amorphous solid has any low-lying modes similar to the phonon-roton mode of liquid ^{4}He, that might suggest Bose-Einstein condensation (BEC) and superflow, or whether it has vibrational modes similar to those of a typical polycrystalline solid as observed in classical amorphous solids.[33–35] This is particularly interesting since a low-energy mode in solid helium in aerogel has recently been reported and identified as the origin of local

superfluidity.[36] In this context, we present measurements of the dynamical structure factor (DSF) of amorphous solid helium.

II. EXPERIMENT

The experiment was performed at the Institut Laue-Langevin on the time-of-flight spectrometer IN5. We used an incident neutron wavelength of 5 Å, which provided a spectrometer energy resolution of 85 μeV.

The sample cell was a cylindrical aluminum container with an inner diameter of 15 mm and a height of 55 mm. The MCM-41 powder sample occupied a volume of 7 cm^3 corresponding to a height of 40 mm in the cell. The upper part of the cell containing bulk He was masked with cadmium. The cell was mounted in a dilution refrigerator built at the ILL that has a base temperature of 40 mK. The cell was filled at $T = 3.8$ K and 80 bars, and the solid sample between the grains of the MCM-41 was formed by the blocked capillary method.

In the present 47-Å pore diameter MCM-41 powder sample, the ratio of the volume in the pores V_P to that between the grains V_{IG} is[32] $V_P/V_{IG} = 0.44$. Thus, approximately 30% of the helium in the beam is in the pores, 70% between the grains. In a 47-Å pore, approximately 30% of the volume in the pore is occupied by the tightly bound amorphous solid layers on the media walls. Thus, in the present MCM-41 sample at 1.6 K when there is liquid in the pores, approximately 80% of the helium in the cell is solid (between the grains and on the pore walls) and only 20% is liquid (in the pores). For this reason, the difference in the scattering intensity arising from the solidification of the liquid to an amorphous solid between 1.6 and 0.05 K is expected to be small, as observed in Figs. 2 and 3.

III. RESULTS

To set the stage, we show the phase diagram of ^{4}He confined in 47-Å pore diameter MCM-41 (Refs. 32 and 40) and in 25-Å mean pore diameter gelsil[38,41,42] in Fig. 1. At low temperature and pressure, liquid ^{4}He is a superfluid in 25-Å gelsil and in 28-Å Folded Sheet Material (FSM), as shown by Yamamoto *et al.*[38] and Taniguchi *et al.*,[37] respectively. In the superfluid phase, the associated Bose-Einstein condensation (BEC) is expected to be connected and continuous across the sample, providing a continuous phase that enables macroscopic superflow. At higher temperature above the superfluid phase in porous media, the liquid forms a localized BEC (LBEC) region in which the BEC is localized to islands. In the LBEC region, the BEC is isolated in patches, is not extended, and there is no macroscopic superflow across the sample.[43,44] The LBEC region lies between the superfluid and normal liquid phases as shown in Fig 1. In 47-Å MCM-41 and 25-Å gelsil, helium solidifies at pressures $p \gtrsim 38$ bars. The liquid-solid boundary in MCM-41 has been determined by cooling the liquid and observing a small reproducible increase in the peak height of the static structure factor $S(Q)$ on solidification.[32] In 25-Å gelsil, it has been determined from pressure drop on solidification.[41] No Bragg peaks were observed in the confined solid,[32] showing that the solid is amorphous with no crystalline regions. In larger pore diameter media, for example in 70-Å

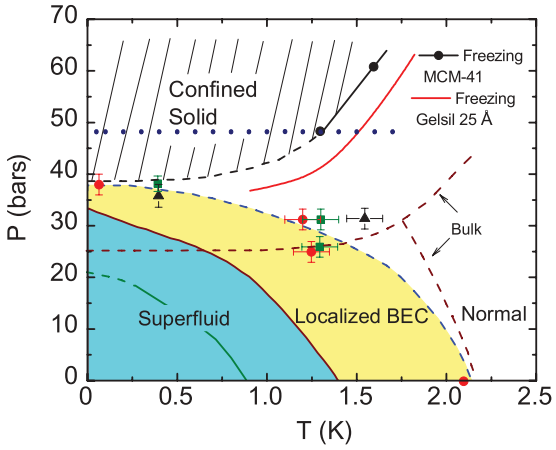

FIG. 1. (Color online) Phase diagram of liquid ^{4}He in MCM-41 (47 Å), gelsil (25 Å), and FSM (28 Å). The superfluid (SF) phase in FSM and in gelsil is at the lower left, the blue region. The green line is the T_c of the SF phase in FSM observed by Taniguchi *et al.* (Ref. 37) and red line the T_c in gelsil observed by Yamamoto *et al.* (Ref. 38). The yellow region shows the localized Bose-Einstein condensation (LBEC) region in gelsil. In the LBEC region, well-defined phonon-roton modes are observed (Refs. 39 and 40), up to but not beyond the pressures and temperatures indicated by the blue dashed line in gelsil and MCM-41 which is taken as the upper limit of the LBEC region. The red solid line is the freezing onset of ^{4}He in gelsil measured by Shirahama *et al.* (Ref. 41). The black solid and dashed lines show the freezing onset of ^{4}He in MCM-41 observed (Ref. 40) from the static structure factor $S(Q)$. The dashed red lines show the phase boundaries in bulk ^{4}He. The blue dots at $p = 46.8$ bars mark the temperatures at which the present measurements were made.

gelsil[45] and aerogel,[46] polycrystalline solid ^{4}He regions are observed.

Figure 2 shows the net DSF of helium in the present sample cell containing MCM-41 at pressure $p = 48.6$ bars. $S(Q,\omega)$ at $Q = 2.0$ Å^{-1} and temperatures $T = 0.05$ and 1.6 K are shown. At $T = 0.05$ K, we expect amorphous solid helium in the MCM-41 pores and polycrystalline solid between the grains of the MCM-41 powder. The inelastic scattering ($\omega > 0$) at $T = 0.05$ K is a sum of $S(Q,\omega)$ from the amorphous solid (30% of the helium sample in the beam) and polycrystalline solid (70% of the helium in the beam). At low ω, the intensity in $S(Q,\omega)$ grows smoothly with ω as expected for scattering from a polycrystal or an amorphous solid in which the density of states $g(\omega)$ is approximately proportional to ω^2 at low ω. There is no indication of any low-energy roton modes or any layer modes as seen in liquid helium in porous media. The roton and layer modes of the liquid in MCM-41 are observed[39,40,47,48] at energies 0.5–0.6 meV and 0.4–0.5 meV at 34 bars, respectively. The DSF in Fig. 2 peaks at $\omega \simeq 1.3$ meV. This is consistent with the peak in the density of states (DOS) of phonons in bulk polycrystalline helium between the grains observed previously.[40,47,48] The large peak at $\omega = 0$ is elastic scattering $S(Q,\omega = 0)$ from the amorphous solid in the pores. The elastic scattering from the polycrystalline solid is confined to Bragg peaks and the **Q** in Fig. 2 has been selected to avoid these Bragg peaks.

In Fig. 2, at $T = 1.6$ K there is new response at low ω in $S(Q,\omega)$ not seen at $T = 0.05$ K. Also, at $T = 1.6$ K the

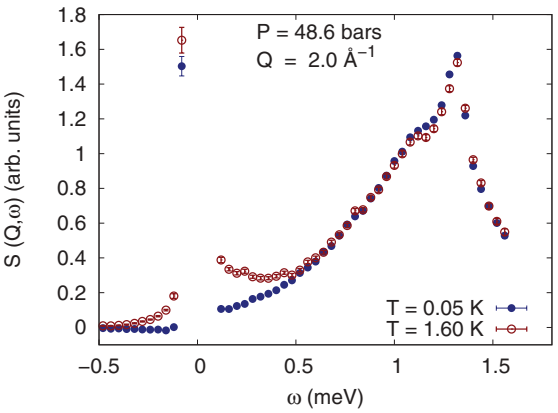

FIG. 2. (Color online) Net $S(Q,\omega)$ at $Q = 2.0$ Å^{-1} of helium in MCM-41 at pressure $p = 48.6$ bars at $T = 0.05$ K (amorphous solid in the pores) and at $T = 1.6$ K (liquid in the pores). $S(Q,\omega)$ includes the scattering from the bulk polycrystalline ^{4}He lying between the grains of the MCM-41. At $T = 0.05$ K, $S(Q,\omega)$ at low ω is approximately proportional to ω^2 characteristic of scattering from a solid. $S(Q,\omega)$ has a peak at $\omega \simeq 1.3$ meV attributed chiefly to the polycrystalline solid. At $T = 1.6$ K, there is liquid in the pores with amorphous solid adjacent on the pore walls. $S(Q,\omega)$ at 1.6 K shows new intensity at low ω characteristic of normal liquid ^{4}He.

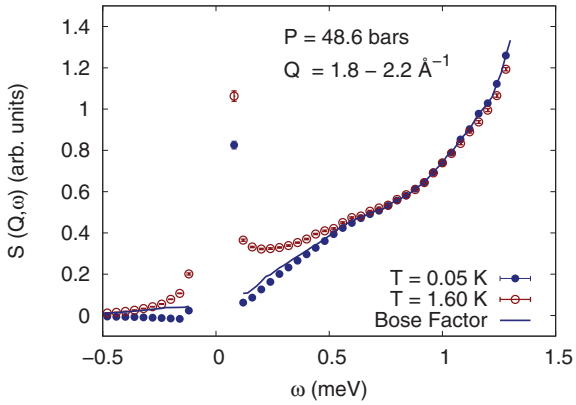

FIG. 3. (Color online) The net $S(Q,\omega)$ as in Fig. 2 integrated over Q between $Q_1 = 1.8$ Å^{-1} and $Q_2 = 2.2$ Å^{-1} as defined in Eq. (1). The line labeled "Bose factor" is the data at $T = 0.05$ K multiplied by the Bose factor $[n_B(\omega) + 1\ ]$ for temperature $T = 1.6$ K where $n_B(\omega)$ is the Bose function. The line displays the change in $S(Q,\omega)$ between 0.05 and 1.6 K expected from thermal contributions alone. At $T = 1.6$ K, thermal contributions to $S(Q,\omega)$ are still clearly small.

intensity in $S(Q,\omega)$ at higher ω ($\omega > 1$ meV) is marginally smaller. At $Q = 2.0$ Å^{-1}, energy transfers $\omega > 1.5$ meV are not observable on IN5 at the present incident neutron energy used. From the phase diagram Fig. 1, we see that the helium in the interior of the MCM-41 pores is liquid at $p = 48.6$ bars and $T = 1.6$ K. The helium in the one-two helium layers tightly bound to the MCM-41 walls remains amorphous solid at $T = 1.6$ K and higher temperatures. Approximately 30% of the helium in the 47-Å MCM-41 pores is in the tightly bound layers adjacent to the pore walls which remains solid at $T = 1.6$ K. Thus, approximately 20% of the total helium sample in the beam melts to liquid between $T = 0.05$ and 1.6 K.

The intensity in $S(Q,\omega)$ at low ω at $T = 1.6$ K is attributed to the normal liquid ^{4}He in the interior of the pores. This $S(Q,\omega)$ is similar to that of bulk normal liquid ^{4}He at 20 bars[49,50] and of confined normal ^{4}He in MCM-41 at 34 bars[48] as we discuss further in the following. That is, $S(Q,\omega)$ is concentrated near $\omega = 0$ with a tail extending out to higher ω, as in normal liquids.[51,52] Particularly, there are no sharp modes in $S(Q,\omega)$ at either 0.05 or 1.6 K characteristic of a Bose-condensed liquid.[48]

Figure 3 shows $S(\omega)$ obtained by integrating $S(Q,\omega)$ over a range of Q values,

$$S(\omega) = \int_{Q_1}^{Q_2} dQ\, S(Q,\omega), \qquad (1)$$

between $Q_1 = 1.8$ Å^{-1} and $Q_2 = 2.2$ Å^{-1}. The purpose of the integration is chiefly to improve the statistical precision of the data, especially at low ω. As in Fig. 2, the additional intensity at low ω at $T = 1.6$ K is attributed to normal liquid ^{4}He in the interior of the pores. The blue line in Fig. 3 shows $S(Q,\omega)$ of solid helium observed at $T = 0.05$ K (bulk polycrystalline helium between the grains and amorphous solid helium in the pores) multiplied by the Bose factor $[n_B(\omega) + 1]$ where $n_B(\omega)$ is the Bose function for $T = 1.6$ K (0.15 meV). The blue line represents the change in $S(Q,\omega)$ of the solid expected when T is increased from 0.05 to 1.6 K if the energies and lifetimes of the modes of the solid remain unchanged. Clearly, thermal effects make only a minor contribution to the observed change in $S(Q,\omega)$ between $T = 0.05$ and 1.6 K, even at low ω for $\omega > 0$. Thus, it is reasonable to attribute the observed large change in $S(Q,\omega)$ at low ω to melting of the amorphous solid in the interior of the pores to a liquid. As in Fig. 2, no sharp or well-defined modes are observed in the integrated $S(Q,\omega)$.

In Figs. 2 and 3, the intensity in the energy range $0.6 < \omega < 1.5$ meV is very similar at $T = 0.05$ K and at 1.6 K. It is marginally smaller at 1.6 K than at 0.05 K, but has a similar energy dependence. Thus, the $S(Q,\omega)$ in this energy range arising from the amorphous solid ($T = 0.05$ K) and the liquid ($T = 1.6$ K) in the interior of the pores appears to be similar but with marginally larger intensity from the amorphous solid.

Figure 4 shows the $S(\omega)$ data arising from the amorphous solid in the pores and the polyscrystalline solid between the grains at $T = 0.05$ K summed over all detectors. The goal is to show that there are no sharply defined modes at $\omega \leqslant 1$ meV at accessible Q values. Rather, $S(\omega)$ increases uniformly with ω as expected for scattering from phonons in a polycrystalline solid. The peak in the data summed over all detectors at 1.3 meV is broader than the peak in $S(Q,\omega)$ at $Q = 2.0$ Å^{-1} shown in Fig. 1. The peak at 1.3 meV is expected to arise chiefly from the polycrystalline solid helium between the grains. Solid helium is a highly anharmonic solid so that there will be substantial anharmonic broadening in the observed $S(Q,\omega)$ and $S(\omega)$. In Sec. IV, we compare $S(Q,\omega)$ and $S(\omega)$ of anharmonic polycrystalline and amorphous solids and provide explicit expressions for the $S(\omega)$ observed from each.

Figure 5 shows the difference between $S(Q,\omega)$ with normal liquid ^{4}He in the pores (at $T = 1.2$ and 1.6 K) and amorphous solid in the pores at $T = 0.05$ K, the latter multiplied by the thermal Bose factor for each temperature as discussed in Fig. 5. This difference is interpreted as the net scattering from the

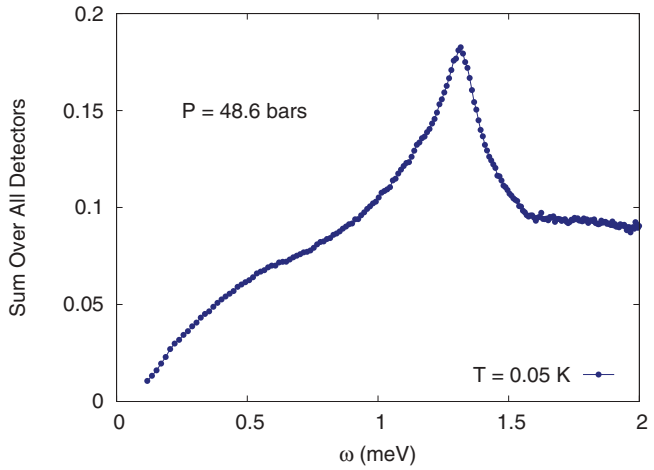

FIG. 4. (Color online) The net $S(\omega)$ as defined in Eq. (1) and shown in Fig. 3 for amorphous solid in the pores and polycrystalline solid between the grains at $T = 0.05$ K summed over all detectors. The sum over all detectors does not show any well-defined modes at low $\omega \leqslant 1$ meV, only an $S(\omega)$ expected from a density of phononlike modes as given by the sum of Eq. (13) describing a polycrystalline solid between the grains and Eq. (20) an amorphous solid in the pores.

normal liquid at low ω. At higher ω ($\omega \geqslant 0.8$ meV), the $S(Q,\omega)$ of the liquid and amorphous solids could be quite similar and the net $S(Q,\omega)$ is not well determined. The net liquid $S(Q,\omega)$ is a smooth function of ω as expected for normal ^{4}He. The $S(Q,\omega)$ also peaks near $\omega = 0$ as observed in classical liquids.[51,52] In contrast, the $S(Q,\omega)$ of normal liquid ^{4}He at SVP ($p \approx 0$) peaks at $\omega \simeq 0.5$ meV. Thus, normal ^{4}He at higher presssure responds much like a classical liquid. The lines in Fig. 5 are fits of a damped harmonic oscillator (DHO)

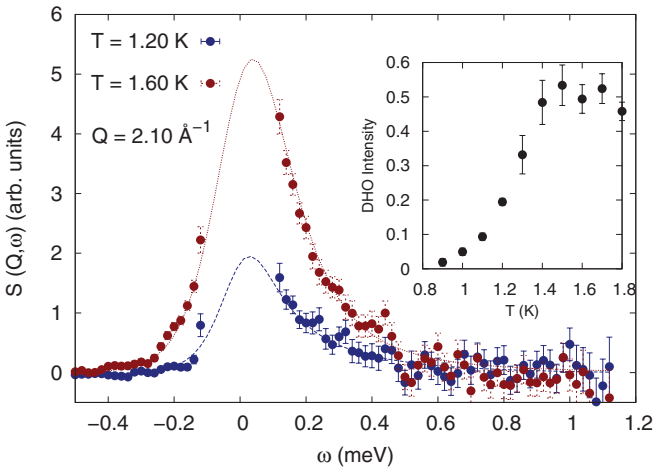

FIG. 5. (Color online) The net $S(Q,\omega)$ of liquid ^{4}He in MCM-41 at $T = 1.2$ and 1.6 K interpreted as normal liquid. The lines are fits of a damped harmonic oscillator (DHO) function. The shape of $S(Q,\omega)$ is independent of temperature. Only the integrated intensity in $S(Q,\omega)$ increases with T (see inset) as more amorphous solid melts to a liquid with increasing temperature. $S(Q,\omega)$ of normal liquid ^{4}He at higher pressure peaks near $\omega = 0$ as observed in classical liquids (Refs. 51 and 52).

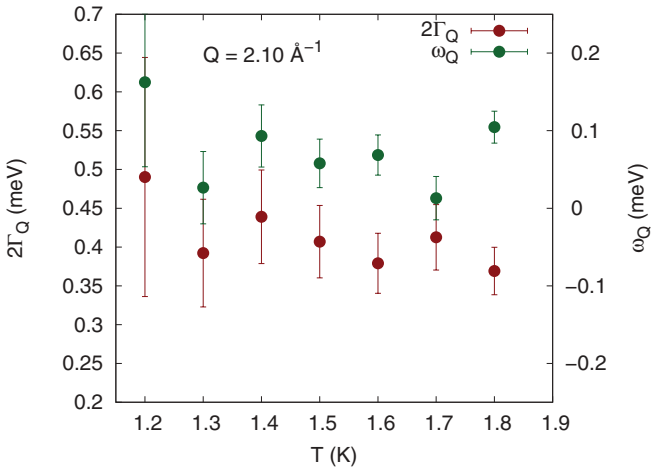

FIG. 6. (Color online) The energy and width (FWHM) parameters of the DHO function that provides the best fit to the normal liquid $S(Q,\omega)$ shown in Fig. 4. The parameters and therefore the shape of the normal liquid $S(Q,\omega)$ are independent of temperature. Only the magnitude of $S(Q,\omega)$ increases with increasing temperature.

function

$$S_1(Q,\omega) = \frac{Z_Q/\pi}{1-\exp(-\hbar\omega/k_BT)} \times \left[\frac{4\omega\omega_Q\Gamma_Q}{\left(\omega^2-\left[\omega_Q^2+\Gamma_Q^2\right]\right)^2+4\omega^2\Gamma_Q^2}\right], \quad (2)$$

to the data with energy ω_Q, width $2\Gamma_Q$, and intensity Z_Q, treated as free fitting parameters. The origin of the DHO is discussed in the Appendixes of Refs. 49 and 53, and the DHO is a standard fitting function in the literature.[50] We found good fits to the data for energies and widths in the DHO function that were independent of temperature within precision (see Fig. 6). Only the weight or intensity in the DHO increased with increasing temperature between 0.8 and 1.4 K. The weight (strictly the product $\omega_Q\Gamma_QZ_Q$ which fluctuates less than Z_Q alone since ω_Q is nearly zero) is shown in the inset of Fig. 5. The increase in intensity with temperature was attributed to the increase in volume of liquid with temperature as the solid melts. The intensity in the liquid $S(Q,\omega)$ reaches a maximum at $T = 1.4$ K, which is interpreted as the temperature when melting of the amorphous solid in the pores is complete. At lower pressure,[48] we also found the energy and width of the normal liquid $S(Q,\omega)$ was independent of temperature over the temperature range investigated ($1.2 < T < 1.8$ K). No physical meaning is attributed to the energy or width in terms of modes. The DHO is only a convenient representation of $S(Q,\omega)$.

Figure 7 shows the net elastic scattering from the helium in the sample cell at $T = 0.05$ and 1.6 K. The top frame of Fig. 7 shows $S(Q,\omega)$ at $Q = 2.2$ Å^{-1} with the elastic peak at $\omega = 0$. The elastic peak in the top frame arises chiefly from the amorphous solid helium in the pores or on the grain surfaces. The elastic scattering from the polycrystalline solid between the grains is confined chiefly to Bragg peaks which are not seen at $Q = 2.2$ Å^{-1}. At $T = 0.05$ K, the pores are full of amorphous solid. At 1.6 K, there is amorphous helium in the first one to two layers on the pore walls only, approximately

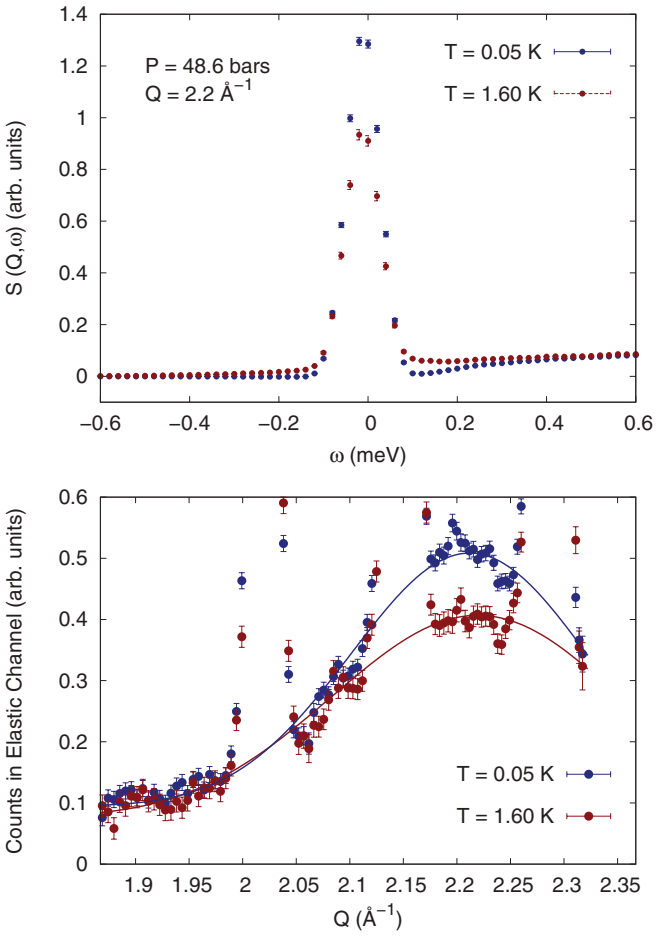

FIG. 7. (Color online) The net elastic scattering from helium in and between the grains of MCM-41 at $T = 0.05$ and 1.6 K. At 0.05 K, there is amorphous solid throughout the pores, at 1.6 K on the pore walls only. Top: $S(Q,\omega)$ with elastic peak at $\omega = 0$ attributed to the amorphous solid. Bottom: $S(Q,\omega = 0)$ vs Q with lines through the amorphous component. Bragg peaks from the bulk hcp polycrystalline solid between the grains can be seen in $S(Q,\omega = 0)$ at $Q = 2.02$ Å^{-1} (1000), 2.15 Å^{-1} (0002), and 2.29 Å^{-1} (1011).

30% of the ^{4}He in the pores. The elastic peak is clearly larger at 0.05 K, indicating more amorphous solid than at 1.6 K. However, the peak is only approximately 20% larger rather than a factor of 2 to 3 as might be expected if only amorphous solid contributes to the peak.

The bottom frame of Fig. 7 shows the elastic scattering $S(Q,\omega)$ at $\omega = 0$ as a function of Q. In this case, Bragg peaks arising from the polycrystalline solid lying between the grains are observed at $Q = 2.02$ and 2.28 Å^{-1}. The blue and red lines in Fig. 7 are guides to the eye through elastic scattering arising from the amorphous solid at $T = 0.05$ and 1.6 K, respectively. Again, the intensity from the amorphous solid is greater at 0.05 K when the pores are filled with amorphous solid than at 1.6 K when there is amorphous solid in one to two layers on the pore walls only. The difference in intensity is comparable to that shown in the top frame of Fig. 7.

Finally, in Fig. 8 we reproduce from Ref. 48 measurements of $S(Q,\omega)$ at lower pressure where there is liquid ^{4}He in the MCM-41 pores at low temperature $T = 0.4$ K. In Fig. 8, we

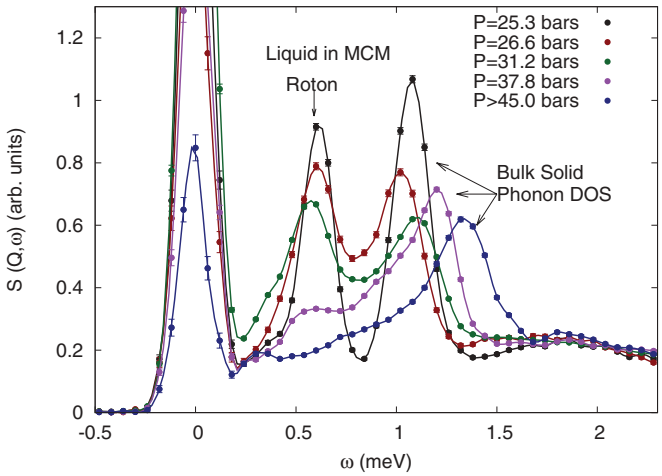

FIG. 8. (Color online) $S(Q,\omega)$ at $Q = 2.1$ Å^{-1} (the roton Q) versus pressure at $T = 0.4$ K from liquid ^{4}He in MCM-41 and bulk solid helium between the grains (from Ref. 48). The intensity arising from the roton of liquid ^{4}He in MCM-41 decreases with increasing pressure until at 37.8 bars there is little or no roton. There is no roton at $p = 45$ bars. The energy of the phonon DOS of the solid increases with increasing pressure.

observe elastic scattering from the amorphous solid layers in the pores at $\omega = 0$, as in the top half of Fig. 7 at $p = 48.6$ bars. The peak at $\omega = 0.6$ meV is the roton mode of the Bose condensed liquid at $Q = 2.1$ Å^{-1}. The intensity in the roton mode clearly decreases with increasing pressure until there is only a very weak mode observed at $p = 37.8$ bars, which is immediately below the solidification pressure. No roton mode is observed at $p \simeq 45$ bars. The decrease in intensity of the phonon-roton modes in the liquid with increasing pressure and disappearance of the mode at the solidification pressure $p \simeq 38$ bars is consistent with no low-energy, liquidlike mode observed here in the amorphous solid at 48.6 bars. The broad peak at higher energy $\omega = 1.0$–1.3 meV in Fig. 8 is scattering from the phonons of the polycrystalline solid lying between the grains. The energy of the peak arising from the phonons increases with increasing pressure as expected for phonons. The broad peak at $\omega \simeq 1.2$ meV at $p = 37.8$ bars shown in Fig. 8 is similar in shape to the peak in $S(Q,\omega)$ at $\omega \simeq 1.3$ meV observed here at 48.6 bars, as seen in Figs. 1 and 4. In each case, this peak is interpreted as arising chiefly from the phonons in the hcp polycrystalline solid between the grains.

IV. DISCUSSION

A. Melting in confinement

Taniguichi and Susuki[54] have recently reported measurements of freezing and melting of helium in a 28-Å pore diameter FSM which is quite similar to the present MCM-41. They observe melting continuously over a wide temperature range, quite different from melting of bulk helium, but freezing over a narrower temperature range. In Fig. 5 above we presented the DSF $S(Q,\omega)$ of normal liquid ^{4}He in the present MCM-41. Particularly, on warming, intensity in the liquid $S(Q,\omega)$ is first observed at $T = 0.9$ K, the intensity grows continuously until 1.5 K, and saturates to a constant value

at 1.5 K (see inset of Fig. 5). We interpret this as onset of melting at 0.9 K and melting complete at 1.5 K. This increase in intensity of the liquid $S(Q,\omega)$ over a wide temperature range is consistent with the continuous melting over a wide temperature range observed by Taniguchi and Susuki. They also observe a very small volume change on freezing, two orders of magnitude below the bulk value. This suggests that the molar volumes of the amorphous solid and liquid in FSM, and probably in the present MCM-41, are nearly identical.

B. Modes in confined liquid ^{4}He

In earlier measurements,[39,40,47,48] we have observed the DSF $S(Q,\omega)$ of liquid ^{4}He in the present MCM-41 and in 25-Å diameter gelsil as a function of pressure and temperature. Both phonon-roton (P-R) and layer modes are observed at low temperature. The intensity in the roton decreases with increasing pressure, as noted above, and with increasing temperature. At $p = 34$ bars, for example, the intensity in the roton disappears at $T = 1.5$ K and a roton is no longer observed above this temperature. The solid circles, squares, and triangles in Fig. 1 show the maximum temperatures and pressures at which P-R modes are observed. At temperatures and pressures above the dashed black line through the data points in Fig. 1, well-defined P-R modes are no longer observed. Since well-defined P-R modes exist when there is Bose-Einstein condensation, the dashed black line is associated with the temperature $T_{\rm BEC}$ at which BEC disappears in liquid ^{4}He confined in these porous media. In 25-Å gelsil, $T_{\rm BEC}$ lies above T_C for superflow as observed in a torsional oscillator.[38] For this reason, the temperature region $T_C < T < T_{\rm BEC}$ is identified as a region of localized BEC with no superflow across the sample as discussed at the beginning of Sec. III.

Equally interesting, the roton energy decreases with increasing pressure, decreasing from $\Delta = 0.74$ meV at saturated vapor pressure (SVP) to approximately $\Delta = 0.55$ meV at 37.8 bars.[39,47] The energy of a single P-R mode can not exceed twice the roton energy[55,56] 2Δ. If the single P-R mode energy exceeds 2Δ, it has sufficient energy to spontaneously decay to two rotons and the mode will be broadened and not observable as a well-defined mode. Thus, at higher pressure, a well-defined liquid P-R mode exists at low energy only, at wave vectors in the phonon region and in the roton region only. For example, at $p \geqslant 38$ bars (at solid pressures), a well-defined P-R mode exists in the liquid at energies $2\Delta \leqslant 1.1$ meV only, i.e., at wave vectors in the phonon region $Q \leqslant 0.6$ meV and in the roton region $1.7 < Q < 2.4$ Å^{-1} only. Thus, even if there were trapped liquid in a solid at higher pressure, we would not observe a complete liquid P-R mode.

In summary, our previous finding that the intensity in the liquid roton mode decreases with increasing pressure and goes to zero at $p \simeq 38$ bars is consistent with the absence of a mode at roton energies in the amorphous solid in the present measurements.

C. Amorphous solid helium

In this section, we compare expressions for the dynamic structure factor (DSF) $S(Q,\omega)$ of an anharmonic polycrystalline and an anharmonic amorphous solid. The goal is to show that we expect the $S(Q,\omega)$ of solid helium in these two structures to be very similar when $S(Q,\omega)$ is integrated over a range of Q values as in Eq. (1). The integrated $S(\omega)$ may be somewhat more sharply peaked as a function of ω in a polycrystalline solid because of the coupling between the scattering wave vector Q and the wave vector q of the phonons in the polycrystalline solid. This coupling limits the number of phonons that can contribute to $S(\omega)$ in a polycrystal. However, because of (1) anharmonic effects which broaden the phonons substantially, (2) the large vibrational displacements of the atoms which make multimode contributions to $S(Q,\omega)$ large, and (3) because we are considering polycrystals rather than single crystals, we expect the difference to be small. To illustrate, we write out the single-mode excitation term $S_1(Q,\omega)$ of $S(Q,\omega)$ for polycrystalline and amorphous solids in the following. Higher-order terms are discussed in the Appendix.

The total $S(Q,\omega)$ is the sum of an elastic scattering term $S_0(Q)$ and a series of inelastic terms representing excitation of single modes, two modes, interference between those modes via anharmonic terms, and higher-order mode processes

$$S(Q,\omega) = S_0(Q,0) + S_1(Q,\omega) + S_{INT}(Q,\omega) + S_2(Q,\omega) + \cdots . \quad (3)$$

In a crystal of N atoms where there is periodic translational symmetry, we express the vibrational displacements $u_l(t)$ of the atoms l from their lattice points R_l as a superposition of waves (phonons) in the crystal of well-defined wave vector q and polarization index λ. With this expression, the product $[Q \cdot u_l(t)]$ that appears in the DSF [see Eqs. (A2) and (A6) in the Appendix] is, for one atom per unit cell,

$$[Q \cdot u_l(t)] = \frac{1}{\sqrt{N}} \sum_{q\lambda} f_{q\lambda} e^{iq\cdot R_l} [Q \cdot \epsilon_{q\lambda}] A_{q\lambda}(t). \quad (4)$$

In Eq. (4) $f_{q\lambda} = (\hbar/2m\omega_{q\lambda})^{1/2}$ where $\omega_{q\lambda}$ is the frequency and $\epsilon_{q\lambda}$ is the polarization vector of the wave and m is the atomic mass. $A_{q\lambda}(t)$ is the mode annihilation operator for the phonon ($q = 1$ to N and $\lambda = 1$ to 3).

In randomly oriented polycrystals of solid helium, we assume that, averaged over the polycrystals,

$$\langle [Q \cdot \epsilon_{q\lambda}]^2 \rangle_{\rm poly} = \tfrac{1}{3} Q^2. \quad (5)$$

We restrict ourselves here to positive ω and low temperature $\hbar\omega \gg kT$ so that the number of the thermally excited phonons is small. In this case, using the substitution (4) and the average (5), the one-phonon component of $S(Q,\omega)$ is

$$S_1(Q,\omega) = I_1(Q) \frac{1}{3N} \sum_{q\lambda} \frac{A(q\lambda,\omega) N \Delta(Q - q - \tau)}{2\pi\omega_{q\lambda}} \quad (6)$$

in which $I_1(Q)$ is the one-phonon weight factor, $I_1(Q) = d^2(Q)(\hbar Q^2/2m)$, $d^2(Q)$ is the Debye-Waller factor, and $A(q\lambda,\omega)$ is the one-phonon response function. In an anharmonic crystal such as solid helium, $A(q\lambda,\omega)$ has the form[53,57]

$$A(q\lambda,\omega) = \frac{8\omega_{q\lambda}^2 \Gamma(q\lambda,\omega)}{\left[-\omega^2 + \omega_{q\lambda}^2 + 2\omega_{q\lambda}\Delta\right]^2 + [2\omega_{q\lambda}\Gamma]^2}, \quad (7)$$

where $\Gamma = \Gamma(q\lambda,\omega)$ is the half-width of the phonon group and $\Delta = \Delta(q\lambda,\omega)$ is a shift in the initial frequency $\omega_{q\lambda}$ arising from anharmonic effects. In solid helium, the $\omega_{q\lambda}$ are typically some positive anharmonic frequencies such as self-consistent harmonic frequencies. The $\Gamma(q\lambda,\omega)$ is large so that $A(q\lambda,\omega)$ is a broad function of ω, especially for phonons near the Brillouin zone edges.[58,59] In a harmonic limit in which $\Gamma \to 0$, the $A(q\lambda,\omega)$ reduces to

$$A(q\lambda,\omega) = 2\pi[\delta(\omega - \omega_{q\lambda}) - \delta(\omega - \omega_{q\lambda})]. \tag{8}$$

For positive energies $\omega > 0$, only the first term in $A(q\lambda,\omega)$ in Eq. (8) contributes to $S_1(Q,\omega)$.

At $p = 48.6$ bars, the one-phonon weight factor $I_1(Q) = d^2(Q)(\hbar Q^2/2m)$ has a broad peak at $Q \simeq 2.3$ Å^{-1}. Thus, for polycrystalline solid helium, we expect $S_1(Q,\omega)$ to be largest at Q values where $I_1(Q)$ has its maximum and at energies where $\omega_{q\lambda}$ is small.

The phonon density of states (DOS) of a harmonic crystal is defined as

$$g(\omega) = \frac{1}{3N}\sum_{q\lambda}\delta(\omega - \omega_{q\lambda}), \tag{9}$$

where the sum is over one complete Brillouin zone. The $S_1(Q,\omega)$ in Eq. (6) is proportional to a modified DOS

$$\tilde{g}_C(\omega) = \frac{1}{3N}\sum_{q\lambda}\frac{1}{2\pi\omega_{q\lambda}}A(q\lambda,\omega) \tag{10}$$

$$\simeq \frac{1}{3N}\sum_{q\lambda}\frac{1}{\omega_{q\lambda}}\delta(\omega - \omega_{q\lambda}), \tag{11}$$

which is the usual DOS weighted by $\omega_{q\lambda}^{-1}$. The $\tilde{g}_C(\omega)$ is the modified DOS that is always observed in neutron scattering measurements.[60] Equation (10) is the general anharmonic DOS that will be observed in $S(Q,\omega)$ of solid helium. The second expression, Eq. (11), for $\tilde{g}_C(\omega)$ holds only in a harmonic approximation (HA). Finally, if we integrate $S_1(Q,\omega)$ over a range of Q values as in Eq. (1), we obtain

$$S_1(\omega) = \int dQ\, S_1(Q,\omega) \tag{12}$$

$$= \left[(2\pi)^3/\Omega\right]\int dQ\, I_1(Q)\tilde{g}_C(\omega)\delta(Q - q - \tau), \tag{13}$$

where we have used $N\Delta(Q) = [(2\pi)^3/\Omega]\delta(Q)$ and $(\Omega = V/N)$ is the volume of the unit cell. In Eqs. (6) and (13), there is a coupling between Q and the phonon wave vector q which means that certain values of q only will contribute to $S_1(\omega)$. A full DOS is not observed. In solid helium, $A(q\lambda,\omega)$ is a broad function in ω, so that only an anharmonic DOS given by Eq. (10), substantially broadened by anharmonic terms, is observed. In Fig. 4, we show an $S(\omega)$ that is integrated over a limited range of Q only. Thus, we expect the corresponding $S_1(\omega)$ to be more sharply localized in ω (representing selected phonons) than the full modified DOS $\tilde{g}_C(\omega)$ given by (10).

In an amorphous solid, the mean positions R_l do not have periodic symmetry. We treat the amorphous solid as a large molecule or as a solid that has a single large unit cell with all N atoms in the unit cell.[61] We express $u_l(t)$ as a superposition of the normal modes of the molecule (numerated by λ, $\lambda = 1$ to $3N$) so that Eq. (4) becomes

$$[Q\cdot u_l(t)] = \frac{1}{\sqrt{N}}\sum_{\lambda} f_\lambda\,[Q\cdot\epsilon_{\lambda l}]\,A_\lambda(t). \tag{14}$$

In this case, the polarization vectors $\epsilon_{\lambda l}$ have an index l. We assume that averaged over the N atoms in the amorphous solid the polarization vectors fulfill

$$\langle[Q\cdot\epsilon_{\lambda l}]\rangle_{\rm amor} = \frac{Q}{\sqrt{3}}. \tag{15}$$

With this assumption, and restricting ourselves to positive ω and low temperatures $\hbar\omega \gg kT$ as before, $S_1(Q,\omega)$ for an amorphous solid reduces to

$$S_1(Q,\omega) = S_M(Q)I_1(Q)\frac{1}{3N}\sum_{\lambda}\frac{1}{2\pi\omega_\lambda}A(\lambda,\omega)$$

$$= S_M(Q)I_1(Q)\tilde{g}_A(\omega), \tag{16}$$

where $S_M(Q) = 1/N\sum_{l,l'}\exp(-iQ\cdot[R_l - R_{l'}])$ is a static structure factor defined in terms of the mean positions R_l of the atoms, $I_1(Q) = d^2(Q)(\hbar Q^2/2m)$ is the one mode intensity as before, $A(\lambda,\omega)$ is the one mode response function of the form Eq. (7), and

$$\tilde{g}_A(\omega) = \frac{1}{3N}\sum_{\lambda}\frac{1}{2\pi\omega_\lambda}A(\lambda,\omega) \tag{17}$$

$$\simeq \frac{1}{3N}\sum_{\lambda}\frac{1}{\omega_\lambda}\delta(\omega - \omega_\lambda) \tag{18}$$

is a modified DOS for the amorphous solid. In a HA, $A(\lambda,\omega)$ reduces to a δ function and Eq. (18) becomes exact. The corresponding $S_1(\omega)$ integrated over a range of Q values is

$$S_1(\omega) = \int dQ\, S_1(Q,\omega) \tag{19}$$

$$= \tilde{g}_A(\omega)\int dQ\, S_M(Q)I_1(Q). \tag{20}$$

There are two important differences between $S_1(\omega)$ for a polycrystal [Eq. (13)] and $S_1(\omega)$ for an amorphous solid [Eq. (20)]. In the amorphous solid, we observe the modified DOS $g_A(\omega)$ directly in $S_1(Q,\omega)$ unaffected by selection of particular modes via a delta function. Also, in the amorphous solid, $S_1(Q,\omega)$ contains an additional factor of $S_M(Q)$, which as $I_1(Q)$, peaks at $Q \simeq 2.3$ Å^{-1}, in solid ^{4}He at $p = 48.6$ bars. Thus, we expect $S_1(Q,\omega)$ in the amorphous solid to be somewhat more sharply peaked in Q (at $Q \simeq 2.3$ Å^{-1}) than in the polycrystal. If $\tilde{g}_C(\omega)$ and $\tilde{g}_A(\omega)$ are similar, we expect the $S_1(\omega)$ for a polycrystal to be somewhat more sharply peaked in ω because of the delta function selection of q values in the polycrystalline case. However, given that $A(\lambda,\omega)$ is itself a broad function of ω, we expect the difference to be small.

In addition to the single mode $S_1(Q,\omega)$, there are higher-mode terms $S_2(Q,\omega)$, $S_3(Q,\omega)$ in (3) which are not negligible in solid helium. The $S_2(Q,\omega)$, which is discussed in the Appendix, is proportional to $I_2(Q) = d^2(Q)(\hbar Q^2/2m)^2$ and has a broad maximum at somewhat higher Q values than $S_1(Q,\omega)$. It peaks in ω at higher ω than $S_1(Q,\omega)$. The chief effect of the higher-order terms is to further broaden $S(Q,\omega)$ and to extend $S(Q,\omega)$ to higher ω.

Also, quite generally, at higher ω we expect the $S(Q,\omega)$ to be independent of phase (liquid or solid) and to become quite similar in polycrystalline, amorphous and liquid helium. Ultimately, the response at high ω arises from high-energy interaction between pairs of atoms via the hard core of the interatomic partial, which will be independent of structure and similar in all three phases. This high-energy region begins at energies greater than the collective mode (e.g., phonon) energies. Thus, we expect $S(\omega)$ of amorphous and crystalline ^{4}He to be similar at high ω as well as at lower ω from the arguments above.

V. CONCLUSION

The dynamical response of amorphous solid helium confined in MCM-41 at 48.6 bars as observed in the dynamical structure factor $S(Q,\omega)$ is a smooth function of energy (ω) characteristic of a solid that has a vibrational density of states approximately proportional to ω^2 at low ω. No sharp excitation at low ω similar to the phonon-roton mode in Bose-condensed liquid helium is observed. The $S(Q,\omega)$ of amorphous and bulk polycrystalline solid helium are similar and broad at Q values around 2 Å^{-1}, as anticipated for a highly anharmonic solid. Above $T = 1$ K, the amorphous solid melts to normal liquid ^{4}He. The $S(Q,\omega)$ at $Q \simeq 2$ Å^{-1} of the normal liquid at 48.6 bars is a broad function that peaks near $\omega \simeq 0$ as in classical liquids, rather than a broad function peaking at a finite ω (e.g., $\omega =$ 0.5 meV) as in (more quantum) normal liquid ^{4}He at $p \simeq 0$.

ACKNOWLEDGMENTS

It is a pleasure to acknowledge the support of the Institut Laue Langevin and O. Losserand and X. Tonon at ILL for valuable assistance with the experiments. This work was supported by the DOE, Office of Basic Energy Sciences, under Contract No. ER46680.

APPENDIX

In this Appendix, we present some background on the dynamic structure factor $S(Q,\omega)$ to support the expressions given in Sec. IV B. We begin with the coherent, intermediate scattering function

$$S(Q,t) = \frac{1}{N}\sum_{l,l'}\langle e^{-iQ\cdot r_l(t)} e^{iQ\cdot r_{l'}(0)}\rangle \tag{A1}$$

$$\approx d^2(Q)\frac{1}{N}\sum_{l,l'} e^{-iQ\cdot[R_l - R_{l'}]} e^{\langle [Q\cdot u_l(t)][Q\cdot u_{l'}(0)]\rangle}, \tag{A2}$$

in which $r_l(t) = R_l + u_l(t)$ where R_l is the mean position of atom l (lattice vector in a crystal) and $u_l(t)$ is the displacement of the atom from R_l at time t, Q is the wave-vector transfer in the scattering and $d^2(Q)$ is the Debye-Waller factor $d^2(Q) = \exp[-Q^2\langle u^2\rangle/3]$ in a cubic crystal. We consider one atom per unit cell and cubic symmetry for simplicity. Equation (A2) omits the anharmonic interference terms. The corresponding DSF is

$$S(Q,\omega) = \frac{1}{2\pi}\int dt\, e^{i\omega t} S(Q,t). \tag{A3}$$

To generate the series Eq. (3), we expand the second exponential in Eq. (A2) in a power series in $\langle [Q\cdot u_l(t)][Q\cdot u_{l'}(0)]\rangle^n$ in the usual way.[53,60] The zero-order term ($n = 0$) is the elastic term. For a crystal in which the R_l has periodic order, the corresponding elastic DSF is

$$S_0(Q,\omega) = d^2(Q)\frac{1}{N}\sum_{l,l'} e^{-iQ\cdot[R_l - R_{l'}]}\delta(\omega)$$

$$= d^2(Q) N \Delta(Q-\tau)\delta(\omega). \tag{A4}$$

The intensity in $S_0(Q,\omega)$ is confined to Bragg peaks at the reciprocal lattice vectors τ. In the present measurements involving bulk polycrystalline solid lying between the grains of the MCM-41, we generally chose wave vectors $\mathbf{Q}$ to avoid the Bragg peaks. In this way, elastic scattering from the polycrystalline solid is not observed. Above 1 K, this is not always easy since above 1 K the polycrystals are continually recrystallizing[32,62] and a Bragg peak may appear during a measurement.

For an amorphous solid, where the mean positions R_l of the atoms do not have periodic order,

$$S_0(Q,\omega) = d^2(Q)\frac{1}{N}\sum_{l,l'} e^{-iQ\cdot(R_l - R_{l'})}\delta(\omega)$$

$$= d^2(Q) S_M(Q)\delta(\omega), \tag{A5}$$

where $S_M(Q)$ is a static structure factor defined by the mean positions R_l of the atoms. The elastic $S_M(Q)$ is not the same as the static structure factor $S(Q)$. We have found that the $S(Q)$ of the amorphous solid is somewhat more sharply peaked in the peak region than that of the liquid, but otherwise the $S(Q)$ of the liquid and amorphous solid are very similar.[32]

The inelastic scattering in which the neutron creates or annihilates a single mode arises from the term proportional to $\langle [Q\cdot u_l(t)][Q\cdot u_{l'}(0)]\rangle$ ($n = 1$) in the expansion of Eq. (A2). The corresponding intermediate DSF is

$$S_1(Q,t) = d^2(Q)\frac{1}{N}\sum_{l,l'} e^{iQ\cdot[R_l - R_{l'}]}\langle [Q\cdot u_l(t)][Q\cdot u_{l'}(0)]\rangle. \tag{A6}$$

For a crystal, we expand $[Q\cdot u_l]$ in Eq. (A6) in terms of phonon modes as in Eq. (4). The single-mode term of $S(Q,\omega)$ for a crystal is then

$$S_1(Q,\omega) = \frac{1}{2\pi}[n_B(\omega)+1] d^2(Q)\frac{1}{N}\sum_{q\lambda} f_{q\lambda}^2 [Q\cdot\epsilon_{q\lambda}]^2$$

$$\times A(q\lambda,\omega) N\Delta(Q-q-\tau), \tag{A7}$$

where $A(q\lambda,\omega)$ is the one-phonon response function given by Eq. (7) in general and by Eq. (8) for a harmonic crystal. Making the assumption Eq. (5) for a polycrystal and in the limit of low temperatures where $n_B(\omega)$ may be neglected, Eq. (A7) reduces to Eq. (9).

For an amorphous solid, we expand the $[Q\cdot u_l]$ in terms of the modes λ of the molecule given by Eq. (14). The resulting $S_1(Q,\omega)$ for an amorphous solid is

$$S_1(Q,\omega) = \frac{1}{2\pi}[n_B(\omega)+1] d^2(Q)\sum_{l,l'} e^{iQ\cdot(R_l - R_{l'})}$$

$$\times \frac{1}{N}\sum_{\lambda} f_\lambda^2 [Q\cdot\epsilon_{\lambda l}][Q\cdot\epsilon_{\lambda l'}] A(\lambda,\omega). \tag{A8}$$

With the assumption Eq. (16) for the $[Q \cdot \epsilon_{\lambda l}]$ and neglecting $n_B(\omega)$, Eq. (A8) reduces to Eq. (17) for amorphous solids. As discussed in Sec. IV B, the coherent $S_1(Q,\omega)$ of an amorphous solid is directly proportional to the DOS $\tilde{g}_A(\omega)$ that would be observed in the incoherent DSF. There is no well-defined wave vector q and therefore no coupling between q and Q as there is in the crystalline case. For an anharmonic solid, we expect $S_1(\omega)$ in the crystalline and amorphous phases to both be substantially broadened by anharmonic effects, which will make the two quite similar.

The two-phonon term $S_2(Q,\omega)$ is the term proportional to $\langle [Q \cdot u_{l'}(t)][Q \cdot u_{l'}(0)]\rangle^2$ in the expansion of Eq. (A2). Substituting the expansion Eq. (4) in this term, we obtain

$$S_2(Q,\omega) = d^2(Q)\frac{1}{2\pi}[n_B(\omega)+1]\frac{1}{2N}\sum_{q_1,\lambda}\sum_{q_2,\lambda} f_2^2 f_1^2 \times [Q\cdot\epsilon_1]^2[Q\cdot\epsilon_2]^2\Delta(Q-q_1-q_2-\tau)A_2(12,\omega), \tag{A9}$$

where

$$[n_B(\omega)+1]A_2(12,\omega) = \int_{-\infty}^{\infty}\frac{d\omega'}{2\pi}[n_B(\omega')+1]A(1,\omega') \times [n_B(\omega-\omega')+1]A(2,\omega-\omega') \tag{A10}$$

and where $1 = q_1\lambda_1$ and $2 = q_2\lambda_2$. For a polycrystalline sample in which Eq. (5) is assumed to hold and in which the temperature is low, $S_2(Q,\omega)$ reduces to

$$S_2(Q,\omega) = d^2(Q)\left(\frac{\hbar Q^2}{2M}\right)^2\frac{1}{2}\left(\frac{1}{3N}\right)^2\sum_{q_1\lambda_1 q_2\lambda_2}\frac{1}{2\pi\omega_1\omega_2} \times A(12,\omega)N\Delta(Q-q_1-q_2-\tau), \tag{A11}$$

where

$$A(12,\omega) = \int\frac{d\omega'}{2\pi}A(1,\omega')A(2,\omega-\omega'). \tag{A12}$$

Since $A(q\lambda,\omega)$ is a broad function, the $A(12,\omega)$ will be an even broader function since $A(12,\omega)$ is a convolution. $S_2(Q,\omega)$ is significant in solid helium and contributes to $S(Q,\omega)$ at higher ω. When $S_2(Q,\omega)$ is significant, we expect $S(\omega)$ given by (1) to be even more similar for amorphous and crystalline solids, especially at higher ω.

[1] E. Kim and M. H. W. Chan, Science **305**, 1941 (2004).
[2] E. Kim and M. H. W. Chan, Nature (London) **427**, 225 (2004).
[3] Ann Sophie C. Rittner and J. D. Reppy, Phys. Rev. Lett. **97**, 165301 (2006).
[4] E. Kim and M. H. W. Chan, Phys. Rev. Lett. **97**, 115302 (2006).
[5] Ann Sophie C. Rittner and J. D. Reppy, Phys. Rev. Lett. **98**, 175302 (2007).
[6] M. Kondo, S. Takada, Y. Shibayama, and K. Shirahama, J. Low Temp. Phys. **148**, 695 (2007).
[7] Y. Aoki, J. C. Graves, and H. Kojima, Phys. Rev. Lett. **99**, 015301 (2007).
[8] P. Gumann, M. C. Keiderling, D. Ruffner, and H. Kojima, Phys. Rev. B **83**, 224519 (2011).
[9] A. D. Fefferman, X. Rojas, A. Haziot, S. Balibar, J. T. West, and M. H. W. Chan, Phys. Rev. B **85**, 094103 (2012).
[10] N. Prokof'ev, Adv. Phys. **56**, 381 (2007).
[11] S. Balibar and F. Caupin, J. Phys.: Condens. Matter **20**, 173201 (2008).
[12] J. T. West, O. Syshchenko, J. Beamish, and M. H. W. Chan, Nat. Phys. **5**, 598 (2009).
[13] S. Balibar, Nature (London) **464**, 176 (2010).
[14] X. Mi and J. D. Reppy, Phys. Rev. Lett. **108**, 225305 (2012).
[15] Z. Nussinov, A. V. Balatsky, M. J. Graf, and S. A. Trugman, Phys. Rev. B **76**, 014530 (2007).
[16] B. Hunt, E. Pratt, V. Gadagkar, M. Yamashita, A. V. Balatsky, and J. C. Davis, Science **324**, 632 (2009).
[17] E. J. Pratt, J. B. Hunt, V. Gadagkar, M. Yamashita, M. J. Graf, A. V. Balatsky, and J. C. Davis, Science **332**, 821 (2011).
[18] J. Day and J. Beamish, Nature (London) **450**, 853 (2007).
[19] J. Day, O. Syshchenko, and J. Beamish, Phys. Rev. B **79**, 214524 (2009).
[20] X. Rojas, A. Haziot, V. Bapst, S. Balibar, and H. J. Maris, Phys. Rev. Lett. **105**, 145302 (2010).
[21] H. J. Maris, Phys. Rev. B **86**, 020502 (2012).
[22] J. R. Beamish, A. D. Fefferman, A. Haziot, X. Rojas, and S. Balibar, Phys. Rev. B **85**, 180501 (2012).
[23] H. Choi, D. Takahashi, K. Kono, and K. E., Science **330**, 1512 (2010).
[24] H. Choi, D. Takahashi, W. Choi, K. Kono, and E. Kim, Phys. Rev. Lett. **108**, 105302 (2012).
[25] Ann Sophie C. Rittner and J. D. Reppy, Phys. Rev. Lett. **101**, 155301 (2008).
[26] D. Y. Kim, H. Choi, W. Choi, S. Kwon, E. Kim, and H. C. Kim, Phys. Rev. B **83**, 052503 (2011).
[27] D. M. Ceperley and B. Bernu, Phys. Rev. Lett. **93**, 155303 (2004).
[28] M. Boninsegni, Nikolay Prokof'ev, and B. Svistunov, Phys. Rev. Lett. **96**, 070601 (2006).
[29] B. K. Clark and D. M. Ceperley, Phys. Rev. Lett. **96**, 105302 (2006).
[30] M. Rossi, D. E. Galli, and L. Reatto, Phys. Rev. B **72**, 064516 (2005).
[31] B. Coasne, S. K. Jain, and K. E. Gubbins, Phys. Rev. Lett. **97**, 105702 (2006).
[32] J. Bossy, T. Hansen, and H. R. Glyde, Phys. Rev. B **81**, 184507 (2010).
[33] K. Suzuki, in *Neutron Scattering, Methods of Experimental Physics*, edited by K. Sköld and D. L. Price (Academic Press, London, 1987), Vol. 23, Chap. 12.
[34] Jens-Boie Suck, Hermann Rudin, Hans Bretscher, Peter Grütter, and Hans-Joachim Güntherodt, Z. Phys. Chem. **157**, 817 (1988).
[35] S. Mentese, J.-B. Suck, and V. Réat, Appl. Phys. A **74**, S969 (2002).

[36]H. Lauter, V. Apaja, I. Kalinin, E. Kats, M. Koza, E. Krotscheck, V. V. Lauter, and A. V. Puchkov, Phys. Rev. Lett. **107**, 265301 (2011).
[37]J. Taniguchi, Y. Aoki, and M. Suzuki, Phys. Rev. B **82**, 104509 (2010).
[38]K. Yamamoto, H. Nakashima, Y. Shibayama, and K. Shirahama, Phys. Rev. Lett. **93**, 075302 (2004).
[39]J. V. Pearce, J. Bossy, H. Schober, H. R. Glyde, D. R. Daughton, and N. Mulders, Phys. Rev. Lett. **93**, 145303 (2004).
[40]J. Bossy, J. V. Pearce, H. Schober, and H. R. Glyde, Phys. Rev. Lett. **101**, 025301 (2008).
[41]K. Shirahama, K. Yamamoto, and Y. Shibayama, Low Temp. Phys. **34**, 273 (2008).
[42]K. Yamamoto, Y. Shibayama, and K. Shirahama, Phys. Rev. Lett. **100**, 195301 (2008).
[43]H. R. Glyde, O. Plantevin, B. Fak, G. Coddens, P. S. Danielson, and H. Schober, Phys. Rev. Lett. **84**, 2646 (2000).
[44]O. Plantevin, H. R. Glyde, B. Fåk, J. Bossy, F. Albergamo, N. Mulders, and H. Schober, Phys. Rev. B **65**, 224505 (2002).
[45]D. Wallacher, M. Rheinstaedter, T. Hansen, and K. Knorr, J. Low Temp. Phys. **138**, 1013 (2005).
[46]N. Mulders, J. T. West, M. H. W. Chan, C. N. Kodituwakku, C. A. Burns, and L. B. Lurio, Phys. Rev. Lett. **101**, 165303 (2008).
[47]J. Bossy, J. V. Pearce, H. Schober, and H. R. Glyde, Phys. Rev. B **78**, 224507 (2008).
[48]J. Bossy, J. Ollivier, H. Schober, and H. R. Glyde, Euro. Phys. Lett. **98**, 56008 (2012).
[49]E. F. Talbot, H. R. Glyde, W. G. Stirling, and E. C. Svensson, Phys. Rev. B **38**, 11229 (1988).
[50]M. R. Gibbs, K. H. Andersen, W. G. Stirling, and H. Schober, J. Phys.: Condens. Mat. **11**, 603 (1999).
[51]K. Sköld, J. M. Rowe, G. Ostrowski, and P. D. Randolph, Phys. Rev. A **6**, 1107 (1972).
[52]W. J. L. Buyers, V. F. Sears, P. A. Lonngi, and D. A. Lonngi, Phys. Rev. A **11**, 697 (1975).
[53]H. R. Glyde, *Excitations in Liquid and Solid Helium* (Oxford University Press, Oxford, 1994).
[54]J. Taniguchi, and M. Suzuki, Phys. Rev. B **84**, 054511 (2011).
[55]L. P. Pitaevskii, Zh. Eksperim. i Teor. Fiz. **36**, 1168 (1959) [Sov. Phys. JETP **9**, 830 (1959)].
[56]H. R. Glyde, M. R. Gibbs, W. G. Stirling, and M. A. Adams, Europhys. Lett. **43**, 422 (1998).
[57]R. A. Cowley, Rep. Prog. Phys. **31**, 123 (1968).
[58]V. J. Minkkiewcz, T. A. Kitchens, G. Shirane, and E. B. Osgood, Phys. Rev. A **8**, 1513 (1973).
[59]T. Markovich, E. Polturak, J. Bossy, and E. Farhi, Phys. Rev. Lett. **88**, 195301 (2002).
[60]S. W. Lovesey, *Theory of Neutron Scattering from Condensed Matter* (Clarendon, Oxford, 1984).
[61]J. M. Carpenter and D. L. Price, Phys. Rev. Lett. **54**, 441 (1985).
[62]C. A. Burns, N. Mulders, L. Lurio, M. H. W. Chan, A. Said, C. N. Kodituwakku, and P. M. Platzman, Phys. Rev. B **78**, 224305 (2008).